Plasmon dispersion on epitaxial graphene studied using high-resolution electron energy-loss spectroscopy

Jiong Lu and Kian Ping Loh*
Department of Chemistry, National University of Singapore, 3 Science Drive 3, Singapore 117543, Singapore

Han Huang, Wei Chen, and Andrew T. S. Wee
Department of Physics, National University of Singapore, 2 Science Drive 3, Singapore 117542, Singapore
(Received 21 July 2009; revised manuscript received 25 August 2009; published 29 September 2009)

We have investigated the momentum-space-dependent behavior of plasmons on epitaxial graphene (EG) using high-resolution electron energy-loss spectroscopy. There are significant differences in the π plasmon behavior for single, bilayer, and 3–4 layer graphene which originate from differences in the in-plane and out-of-plane modes, as well as the different band structures between single-layer and few-layer graphene. The π and $\sigma+\pi$ surface plasmon modes in single-layer EG are recorded at 5.1 and 14.5 eV at small momentum transfer (q); these are redshifted from the values in multilayer EG. In single-layer graphene, a linear dispersion of the plasmon mode is observed, in contrast to the parabolic dispersion in multilayer EG. The overall linear π plasmon dispersion between 4.8–6.7 eV is attributed to the mixing of electronic transitions caused by local field effects, which includes the linear dispersion features resulting from transitions within the "Dirac cone." We also observe that the intensity of the Fuches-Kliewer phonon of SiC and loss continuum of EG varies with the thickness of epitaxial graphene.

DOI: 10.1103/PhysRevB.80.113410 PACS number(s): 79.20.Uv, 71.45.Gm, 34.80.Dp, 68.49.Jk

Graphene, a two-dimensional (2D) carbon atomic sheet connected in a honeycomb lattice, has attracted significant attention both theoretically and experimentally because of its unique electronic structure, high carrier mobilities, and quantum relativistic phenomena.[1–3] 2D graphene exhibits a linear energy dispersion near K, K' points of the Brillouin zone for the electron and hole bands which meet at a single symmetry point. This is markedly different to the conventional 2D semiconductor systems which show a quadratic dependence.[4] Conceptually, useful insights have been obtained by comparing the plasmon behavior of single wall carbon nanotubes to that of graphene sheets especially in the limit when tube radius $\rightarrow\infty$ where the plasmon responses of single sheet graphene and single wall carbon nanotube (SWCNT) converge.[5,6] Moreover, it is instructive to consider how the interlayer interaction affects the graphitic dielectric response. As the interlayer separation increases, the energy-loss function can be viewed as the evolution of plasmon behavior from multilayer graphene to single-layer graphene.[7,8]

High-resolution electron energy-loss spectroscopy (HREELS) and electron energy-loss spectroscopy (EELS) spectra have been collected on the graphitized surface of SiC (0001) by several groups[9–12] For example, Angot *et al.*[9] reported that the π plasmon dispersion of the graphite layer grown on 6H-SiC (0001) was similar to the dispersion relation measured on highly oriented pyrolitic graphite in the energy range of 6–7 eV. Recently, Liu *et al.*[10] studied the dispersion of low-energy sheet plasmon (0.2–2 eV) on single-layer EG. However, the plasmon dispersion has not been considered as a function of the evolution of the thickness of EG. Here, we performed high-resolution electron energy-loss measurements on EG to study how the plasmon behaviors as well as the intensity of the Fuches-Kliewer (FK) phonon of SiC and loss continuum varies with the thickness of the EG. HREELS, which involves the scattering of grazing incidence and low-energy electron from the surface, has much higher surface sensitivity compared to transmission EELS and optical absorption experiments.[13] We select epitaxially grown graphene (EG) on SiC (0001) for study in this work because the layer thickness as well as crystallinity of the epitaxial graphene can be controlled readily by *in situ* annealing. By measuring the angular distribution of the inelastically scattered electrons, the momentum space dispersion of plasmons and nonoptical interband transitions ($q>0$) can be recorded. From the q dependence of the loss function, the features arising from localized or delocalized electronic states can be distinguished directly.[14]

All the measurements were performed using a HREELS spectrometer (SPECS Delta 0.5) mounted in an ultrahigh vacuum (2×10^{-10} Torr base pressure). The energy resolution of the elastic peak was set at 10–15 meV to maximize the signal-to-noise ratio at the spectral regions corresponding to the plasmon loss. With a fixed angle of incidence $\Theta_i=53$ °C with respect to the surface normal, we calculated $q_{\|}$, the parallel momentum transfer to graphene plane from kinematic expression (1), where E_i is incident electron energy, E_{loss} is the measured loss energy, and Θ_s is the different scattering angle. The momentum slit resolution is in the range of 0.03–0.06 Å^{-1},

$$q_{\|}=\frac{\sqrt{2mE_i}}{\hbar}(\sin\Theta_i-\sqrt{1-E_{\text{loss}}/E_i}\sin\Theta_s). \quad (1)$$

EG graphene sample was prepared on a Si-terminated 6H-SiC (0001) crystalline wafer surface by solid-state graphitization.[12,15] First, annealing the silicon-enriched SiC sample at 1100 °C produced a carbon-rich surface layer referred to the literature as the carbon nanomesh.[16,17] After annealing at 1200 °C or higher, monolayer (1200 °C, 2 min), bilayer (1250 °C, 2 min), and 3–4 layers (above

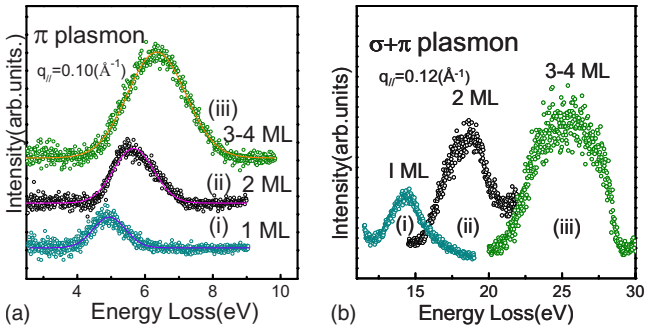

FIG. 1. (Color online) (a) π plasmon peak after background subtraction. The solid line represents a Gaussian fit to the peak. (b) $\sigma+\pi$ plasmon of (i) single-layer EG; (ii) bilayer EG; (iii) 3–4 layer EG. Incident electron energy $E_i=110$ eV; incident angle $\Theta_i=53$ °C.

1300 °C, 2 min) EG films form on top of the carbon nanomesh. The epitaxial graphene thickness was independently verified by low-temperature scanning tunneling microscopy.[15]

Figure 1 shows π and $\sigma+\pi$ plasmons for graphene layers with different thicknesses recorded under identical conditions with the momentum transfer parallel to surface ($q=0.1$ Å^{-1}). As shown, the frequencies of the two collective excitation modes shift to higher energies with simultaneous broadening of the peak as the thickness of the EG layers increases. Here, the π and $\sigma+\pi$ plasmons are presented separately for comparison. In Fig. 1(a), the plasmon spectra taken at $q=0.1$ Å^{-1} show that the π mode, at 5.1 eV in single EG, shifts to 5.6 eV for the bilayer and 6.3 eV for 3–4 layers EG. The frequency of the π mode for single-layer EG agrees with the previous EELS data of SWCNT and free-standing graphene film.[5,6] The 6.3 eV loss peak for the 3–4 layer G, which is close to the π plasmon energy of graphite,[5,8,18] indicates the graphitelike nature of multilayer EG. Accompanying the blueshift, the peak width broadens with increasing number of graphene layers. The width of energy-loss peak for the 3–4 layer EG is 1.71 eV, ~2 times the value of single-layer EG (0.94 eV). The $\sigma+\pi$ mode shown in Fig. 1(b) shifts from 14.5 eV in the single-layer EG to 26 eV in 3–4 layer EG. The width of the $\sigma+\pi$ loss energy peak also becomes broader as the thickness of the epitaxial graphene increases, similar to that of π mode. The π plasmon of 3–4 layer EG contains the out-of-plane loss peak (4.6 eV for free-standing multilayer graphene sheets), which is forbidden in single-layer EG. In addition, the in-plane mode does not occur for single-layer EG or bilayer EG with AB stacking.[5] For the $\sigma+\pi$ mode, the analysis of the plasmon behavior of carbon nanotube provides a good source of reference.[19] The intensity of the out-of-plane mode becomes weaker as the graphene sheet become thinner. Thus, the lower $\sigma+\pi$ plasmon energy centered at 14.5 eV for single-layer EG (similar to SWCNT) can be described as a limiting case when the out-of-plane mode vanishes and only the in-plane mode remains. The broad plasmon peak width in multilayer EG can be explained by responses contributed from both the out-of-plane and in-plane excitations of graphitic origin. The presence of vertical decay channels in

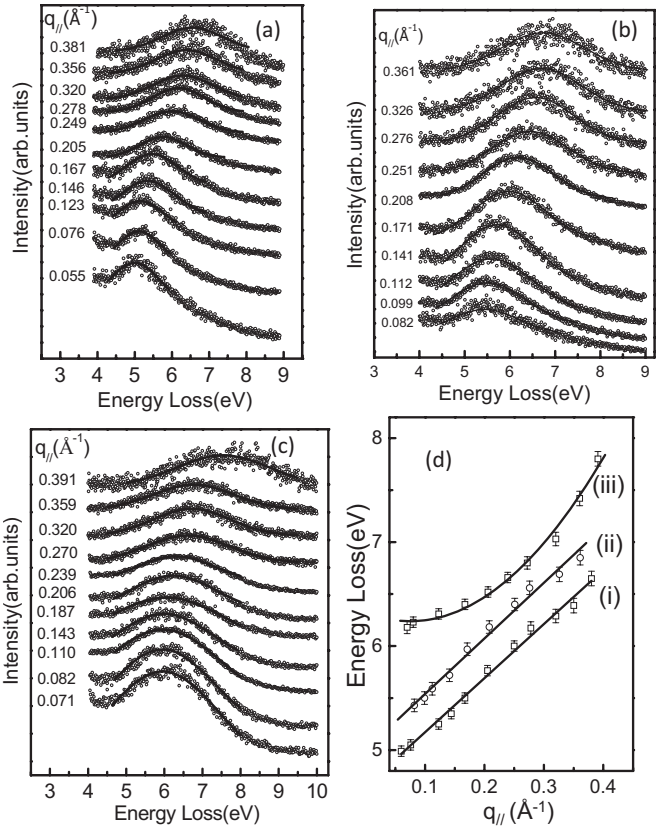

FIG. 2. Measured loss function of (a) single-layer EG, (b) bilayer EG, and (c) 3–4 layer EG from $q=0.05$ Å^{-1} (bottom) to 0.4 Å^{-1} (top) and the dispersion curve for the corresponding EG sample shown in (d), respectively: (i) single-layer EG, (ii) bilayer EG, and (iii) 3–4 layer EG.

multilayer EG causes additional damping of the plasmons, which result in a more diffuse shape for the loss spectrum.[8,20]

Figure 2 displays the k-space positive dispersion of π plasmon energies for graphene of different thicknesses. It can be seen that single-layer graphene exhibits a linear dispersion of the π plasmon energies, as opposed to parabolic dispersion for 3–4 layer graphene. A series of EELS spectra of π plasmons for single-layer EG recorded at different scattering angles is shown in Fig. 2(a). The loss peak can be seen to move to higher loss energy with increasing parallel momentum transfer. From the q dependence of the loss function, it is judged that the dispersive response belongs to a plasma oscillation of delocalized states propagating along the graphene sheet plane. The π plasmon for single-layer EG disperses strongly from 5.1 eV at $q=0.1$ Å^{-1} to 6.7 eV at $q=0.4$ Å^{-1}. The extrapolation of the corresponding π plasmon position to the optical limit ($q\rightarrow 0$) predicts the values to be around 4.82 eV, which agrees with the previous data of SWCNT (Ref. 21) and our experimental result shown in Fig. 3. At $q\rightarrow 0$, the energy-loss peak measured at 4.80 eV matches well with UV adsorption peak at 4.78 eV. Furthermore, linear dispersion of the π plasmon in single-layer EG up to 0.4 Å^{-1} was observed. The plasmon dispersion in the small q limit is predicted to be quadratic in q in the case of the interacting electron gas,[22] namely, $E_{\mathrm{pl}}(q)=E_{\mathrm{pl}}(0)+\alpha\hbar^2/mq^2$, where E_{pl} is the q-dependent plasmon energy and

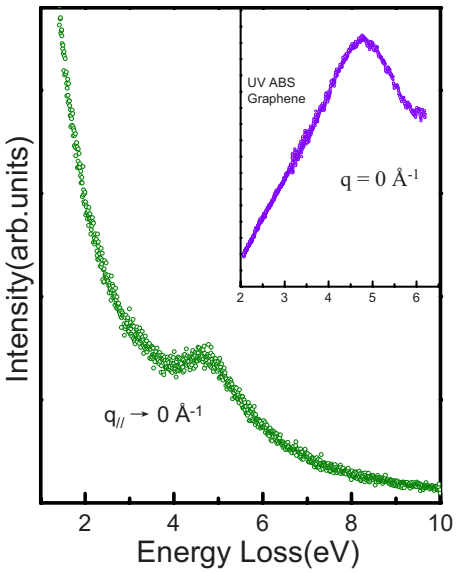

FIG. 3. (Color online) The UV absorption of solution processed graphene (inset) and EELS spectrum of single-layer EG at $q \rightarrow 0$ Å^{-1}.

α is the dispersion coefficient. The experimental result in Fig. 2(d) shows that the parabolic dispersion in 3–4 layers EG is similar to the π plasmon dispersion for graphite. The linear dispersion of single-layer EG may originate from the linear dispersion of "Dirac electron" in graphene. Although the features observed (4–8 eV) are outside the energy range of the linear cone, previous calculation by Kramberger *et al.*[6] reveals that the linear π plasmon dispersion along the vertically aligned SWCNT axis is related to the unique band structure of graphene near the K point. The EELS spectrum can be interpreted as a sum of independent transitions from occupied bands to unoccupied bands which are directly related to the band structure within the bare random-phase approximation (RPA). In the bare loss function, the strong structure due to transitions within the Dirac cone displays the linear dispersion up to 4.0 eV from the K point at 0.5 eV, while the energy-loss peak arising from the transitions near the edge of the Brillouin zone shows quadratic dispersion. Upon the inclusion of crystal local field effects, the quadratic dispersion was transformed into a near linear dispersion as the plasmon response is corrected by considerable contributions from vertical transitions in the Dirac cone. Therefore, the almost linear dispersion for single-layer graphene can be explained by a superposition of the dispersion of the main structure in the bare RPA loss functions, including that resulting from the Dirac cone.

A similar dispersion trend toward higher energy with increasing parallel momentum transfer is observed for single-layer as well as few-layer EG shown in Figs. 2(b) and 2(c). The energy-loss peak at small q recorded on single and few layers EG presents an obvious tail on the high-energy-loss side. The asymmetry of the loss peak may be due either to the excitation of the bulk plasmon or the electron-hole pairs. Even in the $q \rightarrow 0$ case, the plasmon sustains a small degree of damping in contrast to the case of the homogenous electron gas where a finite q is needed for the onset of the electron-hole pair excitation region.

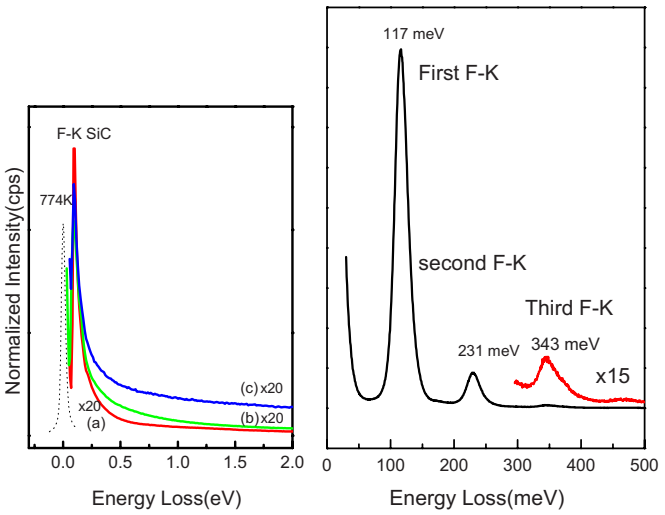

FIG. 4. (Color online) EELS spectra collected in specular direction (E_i=10 eV, incident angle Θ_i=53 °C) for EG with different thicknesses: (a) single-layer EG, (b) bilayer EG, and (c) 3–4 layer EG. The right plot shows the FK phonons of SiC (0001).

The dispersion for EG with thickness less than five layers is positive over the momentum range investigated (0–0.4 Å^{-1}), which is different from surface plasmon dispersion for metals such as Ag and Hg. From the dielectric response of graphite, with increasing q, the main trend of the line shape of Im(ε_M) is a progressive shift of the oscillator strength to higher energies.[8] This behavior is accompanied by a weakening of the electron screening as evidenced by the reduced magnitude of Re(ε_M). These observed changes in $\varepsilon_M(q)$ as a function of q have important consequences on the energy-loss function and the plasmon dispersion. With increasing q, the frequencies of both valence plasmons as well as their effective widths increase. The positive dispersion also can be interpreted by referring to the semimetallic band structure of graphene and graphite. For a single-layer graphene, the symmetry group leads to a degeneracy of the π bands at the K point. The Fermi level intersects the π band at the K point leading to a very small density of states (DOS) at E_F but sharp rise in the DOS above and below E_F. For a finite parallel momentum transfer $q_{\|} \neq 0$, the allowed transitions in K space are no longer vertical, which can be represented by shifting the bands below E_F rigidly by q.[23,24] Thus, the transitions in the energy below the critical energy (E_c) is forbidden, whereas only the energy transition above the E_c is allowed. The whole interband transition would lead to a redshift of the plasmon energy at $q_{\|}$. With increasing $q_{\|}$, (E_c increasing) the band of allowed interband transitions therefore shifts away from the plasmon energy, resulting in a smaller influence on the plasmon energy. Thus, the π plasmon energy is expected to converge to the value determined by free carrier density, giving rise to the positive dispersion observed here.

The unique band structure and density of states of graphene are also reflected in the low-energy-loss range (0–2 eV) shown in Fig. 4. The intensity of FK phonons of SiC decreases as the graphene thickness increases. An intense loss continuum is observed in single, bilayer, and 3–4 layer

EG. The main peak at 117 meV corresponds to the first FK phonon that is typical for the SiC (0001) surface.[11] The second FK phonon peak at 235 meV and third FK phonon peak at 345 meV are clearly resolved before the growth of thicker graphene layers. As the first layer graphene grows on top of the SiC, the intensity of the first FK phonon decreases and the double and triple excitation of FK phonon merge with the energy loss of electron-hole excitation or low-energy sheet plasmon.[10] The loss continuum for graphene is highly intense compared to SiC (0001). Due to the unique band structure and zero band gap of graphene, vertical electronic transitions from zero energy upward are allowed without parallel momentum transfer for small energy excitations in the specular direction, giving rise to the intense loss continuum. Such transitions are forbidden in semiconductors, insulators, and metals. The intensity of loss continuum in 3–4 layers EG is higher than that of single-layer and bilayer EG; this may be due to the three-dimensional band structure of graphite which allows for interlayer coupling and out-of-plane excitation.

In summary, we have measured the wave-vector dependence of plasmon dispersion on epitaxially grown graphene on SiC. A number of intriguing differences are observed in the plasmon loss energies for graphene of different thicknesses. The linear and positive dispersion of π plasmon in single-layer EG reflects the linear dispersion of band structure near the K point in contrast to parabolic dispersion in multilayer EG. In the lower energy-loss region, the intensity of the FK phonon and loss continuum also provides fingerprint profiling of the thickness of the graphene layers. Therefore, we demonstrate that HREELS measurement can be used as a sensitive tool for the determination of the layer thickness of graphene.

The authors acknowledge the NRF-CRP grant of "Graphene Related Materials and Devices" (Grant No. R-143-000-360-281) for financial support.

*Author to whom correspondence should be addressed; chmlohkp@nus.edu.sg

[1] K. S. Novoselov, A. K. Geim, S. V. Morozov, D. Jiang, M. I. Katsnelson, I. V. Grigorieva, S. V. Dubonos, and A. A. Firsov, Science **306**, 666 (2004).
[2] A. K. Geim and K. S. Novoselov, Nature Mater. **6**, 183 (2007).
[3] A. H. Castro Neto, F. Guinea, N. M. R. Peres, K. S. Novoselov, and A. K. Geim, Rev. Mod. Phys. **81**, 109 (2009).
[4] E. H. Hwang and S. Das Sarma, Phys. Rev. B **75**, 205418 (2007).
[5] T. Eberlein, U. Bangert, R. R. Nair, R. Jones, M. Gass, A. L. Bleloch, K. S. Novoselov, A. Geim, and P. R. Briddon, Phys. Rev. B **77**, 233406 (2008).
[6] C. Kramberger, R. Hambach, C. Giorgetti, M. H. Rümmeli, M. Knupfer, J. Fink, B. Büchner, L. Reining, E. Einarsson, S. Maruyama, F. Sottile, K. Hannewald, V. Olevano, A. G. Marinopoulos, and T. Pichler, Phys. Rev. Lett. **100**, 196803 (2008).
[7] A. G. Marinopoulos, L. Reining, V. Olevano, A. Rubio, T. Pichler, X. Liu, M. Knupfer, and J. Fink, Phys. Rev. Lett. **89**, 076402 (2002).
[8] A. G. Marinopoulos, L. Reining, A. Rubio, and V. Olevano, Phys. Rev. B **69**, 245419 (2004).
[9] T. Angot, M. Portail, I. Forbeaux, and J. M. Layet, Surf. Sci. **502-503**, 81 (2002).
[10] Y. Liu, R. F. Willis, K. V. Emtsev, and Th. Seyller, Phys. Rev. B **78**, 201403 (2008).
[11] W.-H. Soe, K.-H. Rider, A. M. Shikin, V. Mozhaiskii, A. Varykhalov, and O. Rader, Phys. Rev. B **70**, 115421 (2004).
[12] T. Langer, H. Pfnür, H. W. Schumacher, and C. Tegenkamp, Appl. Phys. Lett. **94**, 112106 (2009).
[13] M. Rocca, Surf. Sci. Rep. **22**, 1 (1995).
[14] T. Pichler, M. Knupfer, M. S. Golden, and J. Fink, Phys. Rev. Lett. **80**, 4729 (1998).
[15] H. Huang, W. Chen, S. Chen, and A. T. S. Wee, ACS Nano **2**, 2513 (2008).
[16] W. Chen, K. P. Loh, H. Xu, and A. T. S. Wee, Langmuir **20**, 10779 (2004).
[17] W. Chen, H. Xu, L. Liu, X. Y. Gao, D. C. Qi, G. W. Peng, S. C. Tan, Y. P. Feng, K. P. Loh, and A. T. S. Wee, Surf. Sci. **596**, 176 (2005).
[18] J. J. Ritsko and M. Rice, Phys. Rev. Lett. **42**, 666 (1979).
[19] O. Stéphan, D. Taverna, M. Kociak, K. Suenaga, L. Henrard, and C. Colliex, Phys. Rev. B **66**, 155422 (2002).
[20] A. G. Marinopoulos, L. Wirtz, A. Marini, V. Olevano, A. Bubio, and L. Reining, Appl. Phys. A: Mater. Sci. Process. **78**, 1157 (2004).
[21] Y. Murakami, E. Einarsson, T. Edamura, and S. Maruyama, Phys. Rev. Lett. **94**, 087402 (2005).
[22] D. Pines, *Elementary Excitations in Solids* (Benjamin, New York, 1964).
[23] P. Laitenberger and R. E. Palmer, Phys. Rev. Lett. **76**, 1952 (1996).
[24] R. E. Palmer, J. F. Annett, and R. F. Willis, Phys. Rev. Lett. **58**, 2490 (1987).